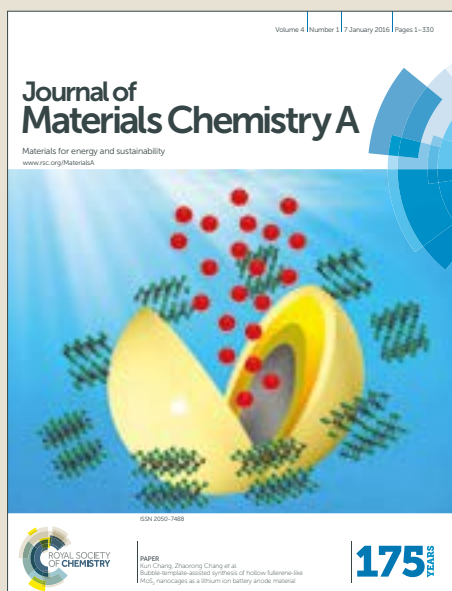


Journal of Materials Chemistry A

Accepted Manuscript



This article can be cited before page numbers have been issued, to do this please use: X. Suo, L. Xia, Q. Yang, Z. Zhang, Z. Bao, Q. Ren, Y. Yang and H. Xing, *J. Mater. Chem. A*, 2017, DOI: 10.1039/C7TA01986F.



This is an Accepted Manuscript, which has been through the Royal Society of Chemistry peer review process and has been accepted for publication.

Accepted Manuscripts are published online shortly after acceptance, before technical editing, formatting and proof reading. Using this free service, authors can make their results available to the community, in citable form, before we publish the edited article. We will replace this Accepted Manuscript with the edited and formatted Advance Article as soon as it is available.

You can find more information about Accepted Manuscripts in the [author guidelines](#).

Please note that technical editing may introduce minor changes to the text and/or graphics, which may alter content. The journal's standard [Terms & Conditions](#) and the ethical guidelines, outlined in our [author and reviewer resource centre](#), still apply. In no event shall the Royal Society of Chemistry be held responsible for any errors or omissions in this Accepted Manuscript or any consequences arising from the use of any information it contains.

Synthesis of Anion-Functionalized Mesoporous Poly(ionic liquid)s *via* a Microphase Separation-Hypercrosslinking Strategy: Highly Efficient Adsorbents for Bioactive Molecules

Xian Suo, Ling Xia, Qiwei Yang, Zhiguo Zhang, Zongbi Bao, Qilong Ren, Yiwen Yang, Huabin Xing*

Received 00th January 20xx,
Accepted 00th January 20xx

DOI: 10.1039/x0xx00000x
www.rsc.org/

The synthesis of porous materials with well-defined pore structure and functionality is centrally important for the development of advanced adsorbents and sensors. In this study, we explored a direct and facile methodology combining microphase separation and hypercrosslinking, and prepare anion-functionalized mesoporous poly(ionic liquid)s (MPILs) with well-developed mesopores. This methodology involved a copolymerization of IL monomers and crosslinkers to create mesopores *via* microphase separation. Additionally, the MPILs were texturally engineered by hypercrosslinking to stabilize/rebuild labile collapsed mesoporous networks and generate a microporosity. Thus, a new family of anion-functionalized MPILs containing amphiphilic long-chain carboxylate ionic liquids (LCC-ILs) were synthesized. These anion-functionalized MPILs exhibited extraordinarily high adsorption capacity (211.45 mg g⁻¹ for tocopherols) and excellent selectivity ($S_{5/ar}$, 8.65; $S_{\beta&\gamma/ar}$, 4.20) for bioactive tocopherol homologues and organic phenolic compounds with high structural similarity, significantly better than those of commercial adsorbents or common MPILs. Additionally, anion-functionalized MPILs demonstrated enhanced carbon dioxide (CO₂) capture performances (28.18 mg g⁻¹ at 0 °C and 1 bar). This study demonstrated the great potential of anion-functionalized MPILs as advanced adsorbents, and facilitates a textural engineering approach to the development of novel porous ionic materials for other applications.

Introduction

Porous polymers with functional surfaces and well-defined pore structures have attracted immense research interest due to their importance in separations, catalysis and energy storage.¹⁻⁵ Mesoporous poly(ionic liquid)s (MPILs) integrate unique properties of ionic liquids (ILs) and porous polymers,⁶⁻⁸ such as high ionic conductivity, tunable physical properties, high surface area, and broad structural diversity, and provide great opportunities for the development of novel porous adsorbents,⁹⁻¹³ membranes,¹⁴⁻¹⁶ catalyst supports,¹⁷⁻¹⁹ and stimuli-responsive materials.²⁰⁻²² The control of pore structure and pore chemistry in MPILs is critical for determining their potential applications. To date, several pore formation strategies have been developed for the fabrication of MPILs with well-defined pore structures. These strategies include a hard template method using sacrificial silica nanoparticles¹² and a soft template method using tri-block copolymer assembly.²³ Recently, due to the unique ionic character of ILs, a template-free ionic complexation strategy *via* acid-base neutralization was presented for facile preparation of MPILs with gradient pore structures was presented.^{13, 14, 20} Additionally, polymerization-induced microphase separation^{24, 25} has been considered an

efficient method for the synthesis of MPILs through a direct radical copolymerization of IL monomers and crosslinkers in nonreactive solvents. Several MPILs containing common hydrophobic ILs and halogen anion-based ILs were successfully prepared using microphase separation.²⁶⁻²⁸ This route uses porogenic solvents as templates and greatly shortens the synthesis period at reduced costs. The selection of a porogenic solvent is critical to pore structure and morphology.²⁹⁻³¹ However, due to the soft and organic nature of MPIL frameworks, MPILs prepared with the aforementioned methods would be confronted with volume shrinkage and pore collapse after template or solvent removal.³²⁻³⁴ Therefore, there is an urgent need to develop an alternative solution to avoid or minimize structural shrinkage, maximize the retention of organic porous matrix, and to realize a textural engineering of MPILs with stable and well-developed mesoporous frameworks.

The functionality and performance of MPILs and ionic materials are dependent on the nature of the ILs, especially on the type of anions. For example, in the separation of drugs and bioactive compounds, ILs with long-chain carboxylate anions or amino acid anions demonstrated superior capacity and molecular selectivity.³⁵⁻⁴¹ Very recently, our group found that the hybrid porous materials containing the hexafluorosilicate anion (SiF₆⁻) showed unprecedented performance for acetylene capture.⁴² However, existing MPILs were limited in common IL monomers, such as hydrophobic ILs and halogen anion-based ILs.^{19, 26, 27} Furthermore, the introduction of functional anions has mostly depended on the post-modification *via* anion exchange. However, this method often

Key Laboratory of Biomass Chemical Engineering of Ministry of Education, College of Chemical and Biological Engineering, Zhejiang University, Hangzhou 310027, China. E-mail: xinghb@zju.edu.cn

† Electronic Supplementary Information (ESI) available. See DOI: 10.1039/x0xx00000x

resulted in changed pore structures and incomplete ion exchange due to steric hindrance, especially for bulky functional anions.^{4, 23, 43} The limited availability and the difficulty of anion-functionalization for MPILs have restricted their applications to primarily carbon dioxide (CO₂) capture^{12, 13} and catalysis.^{18, 19, 27} Applications in separations of drug and bioactive molecules have rarely been reported.⁹ Additionally, although many common porous polymers have been prepared for the separation of CO₂^{3, 44-46} and bioactive molecules,^{47, 48} the design of porous materials with both high capacity and selectivity remains challenging.

Herein, we have explored a facile methodology combining microphase separation and hypercrosslinking to prepare anion-functionalized MPILs. A family of new MPILs containing long-chain carboxylate ILs (LCC-ILs) were prepared. These MPILs possessed stable, well-developed mesopores and adequate functional IL moieties. This method used the copolymerization of IL monomers and crosslinkers to create mesopores *via* microphase separation after template solvent removal. We subsequently employed a textural engineering approach by hypercrosslinking to stabilize/rebuild labile collapsed mesoporous networks and produce new micropores. The prepared anion-functionalized MPILs demonstrated extraordinary adsorption capacity and excellent selectivity to bioactive compounds with high structural similarity and were superior to common MPILs and commercial adsorbents. The anion-functionalized MPILs also exhibited enhanced CO₂ adsorption capacity and good CO₂/N₂ selectivity after hypercrosslinking treatment.

Results and discussion

Fig. 1 depicts the synthetic route for long-chain carboxylate anion-functionalized MPILs. Here, porous copolymers of the 1-ethyl-3-vinylimidazolium-based LCC-ILs and divinylbenzene (DVB) crosslinker are referred to as P(nDVB-EVIMCm)s, and hypercrosslinked MPILs are referred to as HP(nDVB-EVIMCm)s, where *n* represents the used molar ratio of DVB to LCC-ILs, *m* represents the even carbon number of the carboxylate anions and changes from 2 to 16. Porous copolymers synthesized from

equimolar levels of DVB and LCC-ILs are herein referred to as P(DVB-EVIMCm)s or HP(DVB-EVIMCm)s. The molecular structures of LCC-ILs and P(DVB-EVIMCm)s are shown in Figs. S1 and S3, † respectively. And the synthetic route is shown in Fig. S2. †

The IL monomer was introduced into the polymer framework by copolymerization with DVB in a selected porogenic solvent. Under optimized porogenic solvent compositions and solvothermal conditions, microphase separation took place accompanied by crosslinking in the process of the polymerization. Through solvent extraction, MPILs of P(nDVB-EVIMCm)s were produced through the shrinkage of a loose network with unstable pores and collapsed porous structures.

After the copolymerization, some double bonds are inevitably residual in these polymer frameworks, due to limited polymeric activity of the secondary vinyl groups in DVB and steric hindrance in dense domains.⁴⁹ P(nDVB-EVIMCm)s were adequately swollen in a suitable good solvent. The porous polymers were hypercrosslinked using the Friedel-Crafts reaction with anhydrous ferric chloride (FeCl₃) as catalysts but without added crosslinking agents. As a consequence, unstable pore structures in the P(nDVB-EVIMCm)s were covalently arrested *via* the formation of methylene bridges between the pendant vinyl groups and accessible aromatic rings.⁴⁸⁻⁵¹ In this way, HP(nDVB-EVIMCm)s had improved porosity, more permanent mesopores and new micropores when compared with parent polymers, which are vitally important for further application.

Preparation of P(nDVB-EVIMC12)s

It is widely accepted that IL units are functional sites in MPILs, and porosity is considered essential in various application, such as adsorption and catalysis. LCC-ILs have demonstrated extraordinary absorption capacity for acidic gases⁵² and excellent extraction performances for various bioactive compounds and phenols, due to their unique amphiphilic properties and strong hydrogen basicity.^{35-38, 53} However, these properties make the preparation of MPILs challenging with large surface areas and well-defined mesoporous structures.

In this work, a solvothermal method was employed to prepare P(nDVB-EVIMC12)s. The composition of porogenic solvent and solvothermal condition play crucial roles in generating porous structures. To act as a pore template, a porogenic solvent should be a good solvent for monomers and a nonsolvent for the formed polymers. N,N-Dimethylformamide (DMF), acetone, ethyl acetate, tetrahydrofuran (THF) and methyl benzene are popular porogenic solvents for preparing MPILs with hydrophilic or hydrophobic IL monomers.^{4, 26-28, 31} However, in the case of amphiphilic LCC-ILs, all the resultant products using the above mentioned solvents were shown to be nonporous copolymers (Table S1, entry 5†). Interestingly, the polar solvent of acetonitrile (MeCN), which is an appropriate solvent for LCC-ILs in forming non-aqueous lyotropic ionic liquid crystals,³⁶ could result in a structured porosity. The sample of P(DVB-EVIMC12) synthesized in MeCN from equimolar DVB and 1-ethyl-3-vinylimidazolium laurate ([EVIM][C₁₁COO]) exhibited satisfactory surface area (evaluated by BET equation, denoted as S_{BET} , 247 m² g⁻¹), large total pore volume (V_{total} , 0.360 cm³ g⁻¹) and adequate IL content (1.01 mmol g⁻¹) (Table1, entry7). As shown in Fig. 2A, the sample displayed a type IV isotherm with

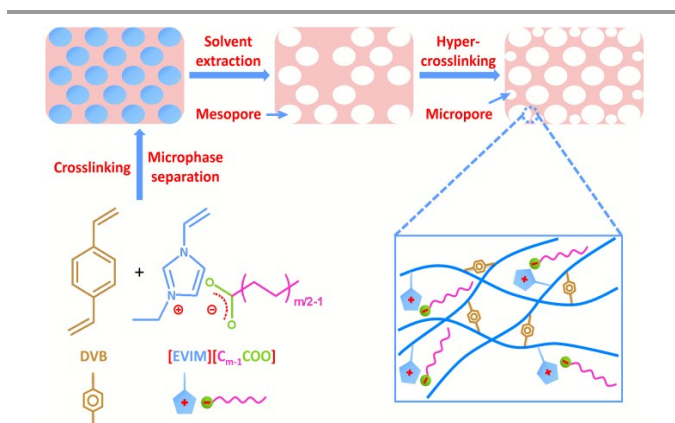


Fig. 1 Synthetic route for anion-functionalized MPILs (P(nDVB-EVIMCm)s) and hypercrosslinked MPILs (HP(nDVB-EVIMCm)s).

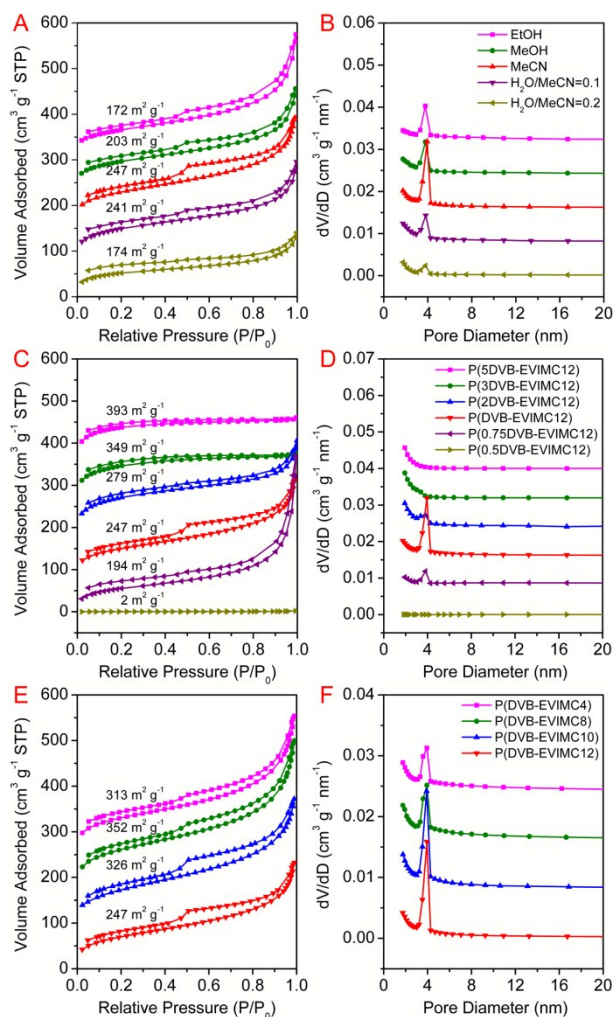


Fig. 2 N₂ adsorption/desorption isotherms (A, C, E) and pore size distributions (B, D, F) of prepared polymers. (A, B) P(DVB-EVIMC12) synthesized in various solvents, (C, D) P(nDVB-EVIMC12)s and (E, F) P(DVB-EVIMCm)s. The isotherms were offset by 80, 160, 240 and 320 cm³ g⁻¹, respectively, along with the vertical axis for clarity, except for P(0.75DVB-EVIMC12); and the pore size distributions were offset by 0.008, 0.016, 0.024, 0.032 and 0.040 cm³ g⁻¹ nm⁻¹, and each of them was estimated by BJH model from a desorption branch of the isotherm.

an evident hysteresis loop of type H2 in the relative pressure (P/P_0) range from 0.42 to 0.90, reflecting the existence of mesopores. The corresponding pore size distribution was displayed in Figs. 2B and S4A.† Thus, this type of porous material showed significant potential for excellent adsorption performance. MPILs of P(DVB-EVIMC12) were also obtained using ethanol (EtOH) (S_{BET} , 172 m² g⁻¹; V_{total} , 0.386 cm³ g⁻¹) and methanol (MeOH) (S_{BET} , 203 m² g⁻¹; V_{total} , 0.326 cm³ g⁻¹) as porogenic solvents. The content of 1-ethyl-3-vinylimidazolium laurate ([EVIM][C₁₁COO]) was moderate (0.83 and 0.74 mmol g⁻¹, Table S1, entries 1 and 2, † respectively). Additionally, we found that the introduction of water into the MeCN solution significantly decreased the surface areas and IL contents of prepared MPILs (Figs. 2A and B; Table S1, entries 3 and 4†). Therefore, pure MeCN was selected as the porogenic solvent

for further exploration.

The ratio of DVB to IL monomer had a significant impact on the porous structure and composition of MPILs. As shown in Figs. 2C, D, and S4B, † the equivalent molar ratio of DVB and [EVIM][C₁₁COO] was an optimal condition to synthesize MPILs with well-developed mesopores and sufficient IL contents. In the Fig. 2C, the sample of MPILs prepared with different molar ratios (n) of DVB to [EVIM][C₁₁COO] is herein named as P(nDVB-EVIMC12)s. At a low DVB-to-IL ratio, P(0.5DVB-EVIMC12) exhibited a nonporous structure. N₂ sorption isotherms of P(0.75DVB-EVIMC12) exhibited a slight hysteresis loop, indicating some mesopores, and displayed a sharp rise at high P/P_0 above 0.80, which is indicative of some macropores. This polymer exhibited wide pore size distributions with a mean mesopore size of 16.0 nm (Table S2, entry 2; Fig. S4B †). At an equivalent molar ratio of DVB and [EVIM][C₁₁COO], well-developed mesopores were observed in the sample of P(DVB-EVIMC12). When the molar ratio of DVB-to-IL was increased from 1:1 to 5:1, the S_{BET} values of the MPILs increased from 247 to 393 m² g⁻¹ (Fig. 2C), whereas the corresponding average pore sizes dropped from 6.8 to 2.7 nm (Table 1, entry 7, and Table S2, entries 3 to 5, † respectively), and the IL content dropped from 1.01 to 0.31 mmol g⁻¹. Additionally, P(2DVB-EVIMC12) showed a type I isotherm with a faint type IV character, indicating the coexistence of abundant micropores and few mesopores. P(3DVB-EVIMC12) and P(5DVB-EVIMC12) presented type I isotherms on typical of micropores. Furthermore, the reaction temperature, time and the initiator dosage influenced the textural properties of the prepared P(DVB-EVIMC12) (Table S3†). For example, the sample obtained at 60 °C had a very low S_{BET} value of 31 m² g⁻¹, and a significantly improved porosity appeared at 80–100 °C. Detailed results are listed in the Table S3. †

Synthesis and characterization of P(DVB-EVIMCm)s with different carboxylate anions

The synthesis strategy was successfully applied to the preparation of a family of P(DVB-EVIMCm)s (their molecular structures are shown in Fig. S3†). All P(DVB-EVIMCm)s (m = 2, 4, 6, 8, 10, 12, 14, and 16) demonstrated well-developed mesoporosities and IL contents larger than 0.78 mmol g⁻¹ (Figs. 2E and F; Fig. S5 and Table S4†). The detailed textural parameters are listed in Tables 1 and S4. † For example, P(DVB-EVIMC10) had a high S_{BET} value of 326 m² g⁻¹, a large V_{total} value of 0.452 cm³ g⁻¹, and an adequate IL content of 1.02 mmol g⁻¹ (Table 1, entry 5).

For the preparation of P(DVB-EVIMCm)s with the carbon number of carboxylate anions larger than 12, we found that EtOH was better porogenic solvent, due to the enhanced hydrophobic properties of the corresponding LCC-ILs. When EtOH was used in the copolymerization, P(DVB-EVIMC14) and P(DVB-EVIMC16) showed well-developed porosities (283 m² g⁻¹, 0.482 cm³ g⁻¹ and 360 m² g⁻¹, 0.620 cm³ g⁻¹, respectively, Table S4, entries 4 and 6†).

The scanning electron microscopy (SEM) micrographs (Figs. 3A and B) of P(DVB-EVIMC12) presented an apparent foam structure with a morphology of sponge-like aggregations, indicating high porosity. The primary irregular particles with tens of nanometers in size were interconnected with each other to form a crosslinked framework with the pore size, which ranges from several to

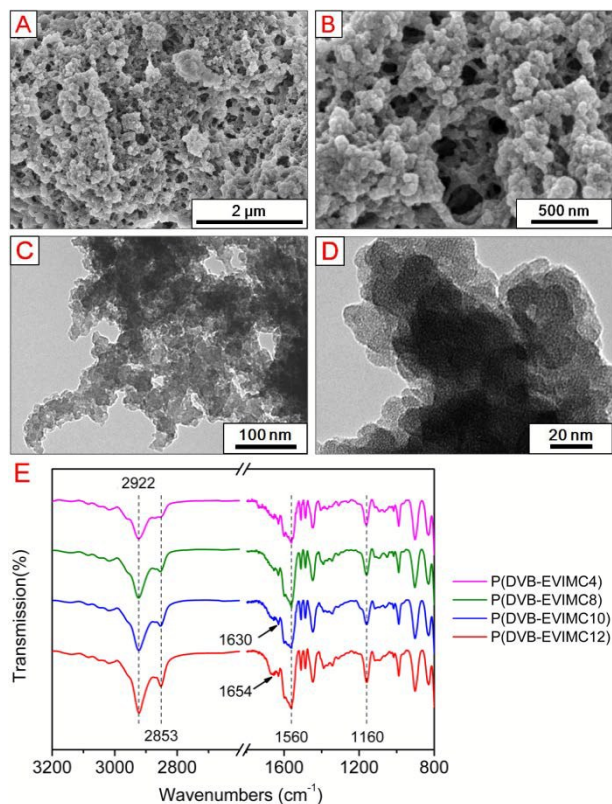


Fig. 3 (A) and (B) SEM micrographs of P(DVB-EVIMC12), (C) and (D) TEM images of P(DVB-EVIMC12), (E) FTIR spectra of representative P(DVB-EVIMCm)s.

hundreds of nanometers. These macropores provided channels for fast solute diffusion. In accordance with N_2 sorption, the presence of disordered mesopores distributed within the copolymer particles was confirmed by the transmission electron microscopy (TEM) images (Figs. 3C and D). Such a hierarchical structure promotes substrate diffusion and adsorption. Other P(DVB-EVIMCm)s had similar hierarchical structures and morphologies as P(DVB-EVIMC12) (Fig. S6[†]).

The obtained copolymers were chemically characterized by Fourier transform infrared spectroscopy (FTIR) to identify their chemical composition. As shown in Fig. 3E, the peak at 1160 cm^{-1} was the characteristic absorption peak of the C-N covalent bond corresponding to substituted N3 in imidazolium-based ILs.⁴³ The peaks at 1654 and 1630 cm^{-1} were assigned to the imidazole ring skeleton. Additionally, the $-\text{COO}^-$ group of carboxylate anions was observed at 1560 cm^{-1} .⁵⁴ The peaks at 2922 and 2853 cm^{-1} were attributed to the saturated C-H group stretching vibrations of carboxylate anions and other aliphatic chains.^{26, 28} Clearly, these results suggested the successful introduction of the IL moieties into the polymeric framework. According to the thermogravimetric analysis (TGA) results shown in Table S5 and Fig. S6,[†] P(DVB-EVIMCm)s exhibited apparently higher stability than the corresponding monomers [EVIM]_m-COO, which was attributed to the crosslinked structure of the copolymer. The onset decomposition temperature of decomposition of P(DVB-EVIMC12)

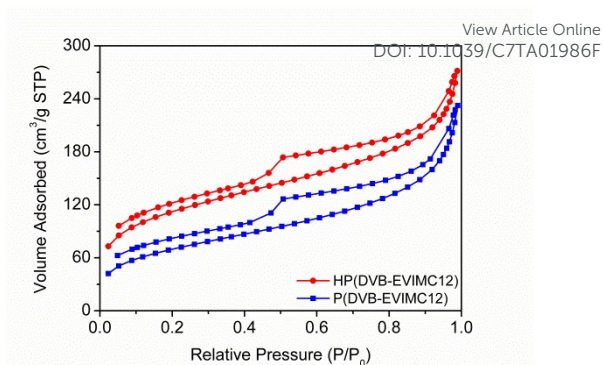


Fig. 4 N_2 adsorption-desorption isotherms of P(DVB-EVIMC12) synthesized in MeCN and corresponding HP(DVB-EVIMC12).

was up to $220\text{ }^\circ\text{C}$ as derived from the decomposition of ILs. Above this temperature, major weight loss roughly started at $350\text{ }^\circ\text{C}$, due to the degradation of the DVB polymeric framework.³¹

In brief, we demonstrated a facile and viable synthesis strategy for the fabrication of P(DVB-EVIMCm)s. Anion-functionalized LCC-ILs were covalently bound onto a crosslinked polymeric matrix. This method prevents the occurrence of tedious and incomplete anion exchange from halogen anions, and prevents the plugging of porous channel due to the introduction of bulky anions.

Synthesis and textural properties of hypercrosslinked P(DVB-EVIMCm)s

Hypercrosslinking is a simple approach to generate micropores and stabilize polymer nanostructures.^{50, 55} In recent years, many hypercrosslinked materials have been prepared.^{34, 44, 50, 56, 57} However, few examples of hypercrosslinking have involved with IL systems.⁵⁸⁻⁶² In this work, to produce hypercrosslinked MPILs (referred to as HP(DVB-EVIMCm)s), the Friedel-Crafts reaction was conducted with the precursor materials (*i.e.*, P(DVB-EVIMC12)). All resultant polymers exhibited apparently enhanced micro- and mesoporosities. As shown in Fig. 4, there were visible differences between P(DVB-EVIMC12) and HP(DVB-EVIMC12). At a relatively lower P/P_0 , the N_2 adsorption capacity of P(DVB-EVIMC12) was significantly enhanced after hypercrosslinking treatment, whereas the pore size distribution of HP(DVB-EVIMC12) demonstrated moderate increase in smaller pore sizes compared with P(DVB-EVIMC12) (Fig. S8[†]). This was due to the newly developed micro- and mesoporosities. Detailed textural parameters for P(DVB-EVIMCm)s and HP(DVB-EVIMCm)s are listed in Table 1. When compared with P(DVB-EVIMC12), HP(DVB-EVIMC12) showed increased S_{BET} and V_{total} (S_{BET} : 386 vs. $247\text{ m}^2\text{ g}^{-1}$; V_{total} : 0.420 vs. $0.360\text{ cm}^3\text{ g}^{-1}$; Table 1, entries 7 and 8). The micropore surface area (S_{micro}) and micropore pore volume (V_{micro}) values increased several-fold prominently enlarged from 14 (P(DVB-EVIMC12)) to $58\text{ m}^2\text{ g}^{-1}$ (HP(DVB-EVIMC12)) and 0.006 to $0.030\text{ cm}^3\text{ g}^{-1}$, respectively. These results indicated that more micropores were formed in the hypercrosslinked network. For the mesoporous structures, after hypercrosslinking treatment on P(DVB-EVIMC12), the external surface area (S_{ext}) values distinctly improved from 233 to $328\text{ m}^2\text{ g}^{-1}$, and pore volume of the mesopores (derived from BJH model, V_{BJH})

Table 1 Textural parameters of several P(DVB-EVIMCm)s^a and the corresponding HP(DVB-EVIMCm)s^b after hypercrosslinking treatmentView Article Online
DOI: 10.1039/C7TA01986F

Entry	Sample	S_{micro}^c $\text{m}^2 \text{g}^{-1}$	V_{micro}^c $\text{cm}^3 \text{g}^{-1}$	S_{ext}^d $\text{m}^2 \text{g}^{-1}$	V_{BJH}^e $\text{cm}^3 \text{g}^{-1}$	D_{BJH}^e nm	S_{BET}^f $\text{m}^2 \text{g}^{-1}$	V_{total}^g $\text{cm}^3 \text{g}^{-1}$	IL content ^h mmol g^{-1}
1	P(DVB-EVIMC4)	42	0.021	271	0.435	7.9	313	0.486	0.90
2	HP(DVB-EVIMC4)	88	0.044	306	0.430	7.4	393	0.512	0.85
3	P(DVB-EVIMC8)	34	0.017	318	0.472	7.4	352	0.525	1.00
4	HP(DVB-EVIMC8)	70	0.034	356	0.483	7.1	426	0.563	0.91
5	P(DVB-EVIMC10)	19	0.009	308	0.412	6.4	326	0.452	1.02
6	HP(DVB-EVIMC10)	77	0.040	355	0.431	6.2	432	0.514	1.03
7	P(DVB-EVIMC12)	14	0.006	233	0.330	6.8	247	0.360	1.01
8	HP(DVB-EVIMC12)	58	0.030	328	0.349	5.5	386	0.420	1.02

^a Polymers served as precursors synthesized with 2 wt% AIBN in MeCN at 80 °C for 24 h. ^b Hypercrosslinked porous polymers via the Friedel-Crafts reaction, prepared with 5 wt% anhydrous FeCl₃ in EtOH at 80 °C for 24 h. ^c Micropore surface area and volume estimated by *t*-plot method. ^d External surface area derived from *t*-plot method. ^e Mesopore volume and mean mesopore diameter calculated from BJH model. ^f BET surface area evaluated from N₂ adsorption isotherm in relative pressure (*P*/*P*₀) from 0.05 to 0.30. ^g Total pore volume at relative pressure (*P*/*P*₀) = 0.990. ^h Loading of IL on the polymer and determined from the elemental analysis.

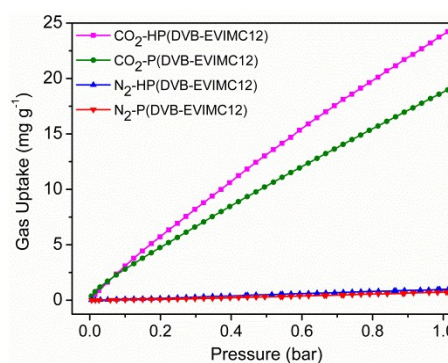
Table 2 Gas sorption properties of several P(DVB-EVIMCm)s and the corresponding HP(DVB-EVIMCm)s

Entry	Sample	CO ₂ uptake ^a mg g^{-1}	N ₂ uptake ^a mg g^{-1}	IAST selectivity ^b (equimolar)
1	P(DVB-EVIMC4)	20.33	0.82	27.18
2	HP(DVB-EVIMC4)	23.10	0.94	26.77
3	P(DVB-EVIMC8)	21.35	0.90	25.54
4	HP(DVB-EVIMC8)	23.16	0.97	26.47
5	P(DVB-EVIMC10)	20.26	0.85	22.75
6	HP(DVB-EVIMC10)	25.26	0.93	28.72
7	P(DVB-EVIMC12)	18.98 (28.18) ^c	0.73 (1.52)	27.63 (22.19)
8	HP(DVB-EVIMC12)	24.22 (33.20)	1.00 (1.91)	26.13 (22.87)

^a Measured at 25 °C and 1 bar. ^b IAST selectivity calculated at 25 °C and 1 bar. ^c The data in round brackets obtained at 0 °C and 1 bar.

values slightly increased from 0.330 to 0.349 $\text{cm}^3 \text{g}^{-1}$. Furthermore, the mean mesopore diameter (D_{BJH}) values declined from 6.8 nm (P(DVB-EVIMC12)) to 5.5 nm (HP(DVB-EVIMC12)). The enhanced micro- and mesoporosities of P(DVB-EVIMCm)s were attributed to the hypercrosslinking treatment. Methylene bridges were formed between the pendant vinyl groups with neighboring benzene rings via the Friedel-Crafts reaction. New micropores were generated, and labile collapsed pores were rebuilt into stable pore networks (Fig. 1). The P(DVB-EVIMCm)s and HP(DVB-EVIMCm)s had nearly the same IL contents (Table 1, entries 1 to 8), which verified that the IL moieties were preserved. And it was not possible to visualize distinct changes in the sponge-like morphology or abundant disordered mesoporosity after hypercrosslinking treatment, based on the SEM and TEM images (Figs. S9 and S10[†]). Therefore hypercrosslinking by the Friedel-Crafts reaction provided an easy and efficient way to prepare MPILs with well-developed micro-mesoporous structures. Through the textural engineering, new micropores were created and stable mesopores were rebuilt, which will enable enhanced sorption capacities for gas separation.

CO₂ capture

**Fig. 5** Gas adsorption isotherms of P(DVB-EVIMC12) and HP(DVB-EVIMC12) at 25 °C for CO₂ and N₂.

Many efforts have been devoted to fabricating porous adsorbents for CO₂ capture.⁶³ In this work, the performances of anion-functionalized P(DVB-EVIMCm)s and HP(DVB-EVIMCm)s for CO₂ capture were evaluated. As summarized in Table 2, P(DVB-EVIMCm)s and HP(DVB-EVIMCm)s with sufficient porosity and adequate IL contents exhibited enhanced CO₂ uptake capacity and

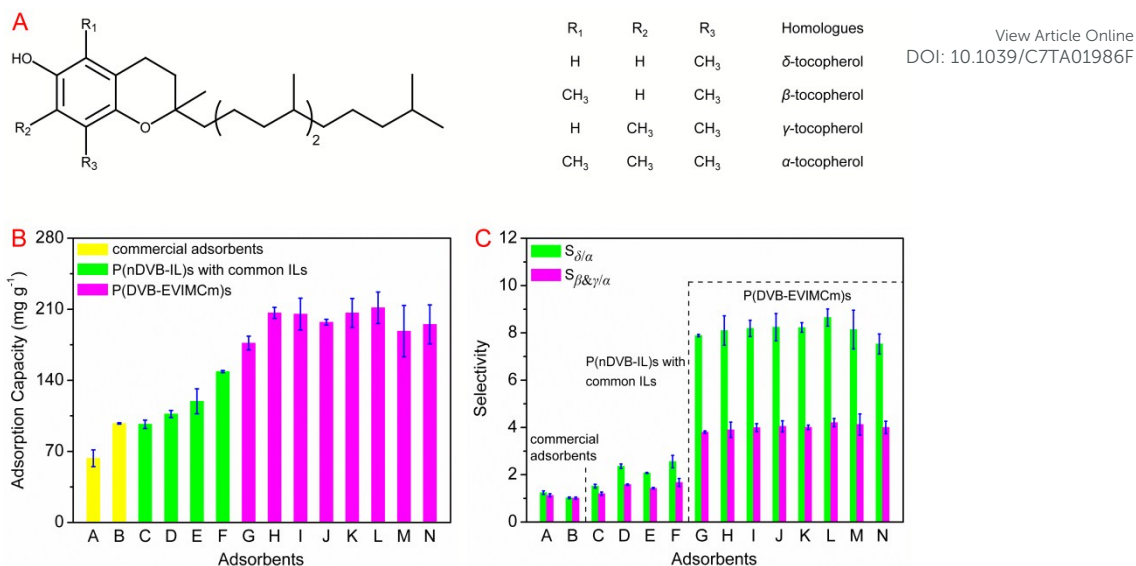


Fig. 6 (A) Molecular structures of tocopherol homologues. (B) Adsorption capacity and (C) selectivity of mixed tocopherols in heptane by commercial adsorbents, P(nDVB-IL)s with common ILs and P(DVB-EVIMCm)s at 25 °C for 24 h. Adsorbents: A. Amberlite XAD-4 B. Amberlite 717 C. P(2DVB-EVIMTf₂N) D. P(2DVB-EVIMBr) E. P(2DVB-EVIMPF₆) F. P(2DVB-EVIMBF₄) G. P(DVB-EVIMC2) H. P(DVB-EVIMC4) I. P(DVB-EVIMC6) J. P(DVB-EVIMC8) K. P(DVB-EVIMC10) L. P(DVB-EVIMC12) M. P(DVB-EVIMC14) N. P(DVB-EVIMC16). All values are mean of three measurements.

good CO₂/N₂ selectivity. At 1 bar, the CO₂ uptakes by P(DVB-EVIMC12) reached 18.98 mg g⁻¹ (25 °C) and 28.18 mg g⁻¹ (0 °C) with remarkable CO₂/N₂ selectivities (22.19–27.63) for equimolar CO₂/N₂ mixture based on ideal adsorbed solution theory (IAST) calculation (Table 2, entry 7). Moreover, the regeneration experiments indicated a good reusability of P(DVB-EVIMC10) at six cycles of CO₂ uptake (Fig. S11 †). After hypercrosslinking treatment, HP(DVB-EVIMCm)s with well-developed porous structure demonstrated a significantly enhanced CO₂ uptake capacity compared with P(DVB-EVIMCm)s (24.22 vs. 18.98 mg g⁻¹ at 25 °C and 33.20 vs. 28.18 mg g⁻¹ at 0 °C and 1 bar, Table 2, entries 7 and 8). The adsorption isotherms of CO₂ on both MPILs are shown in Fig. 5, and an improved capture ability is observable by comparing P(DVB-EVIMC12) and HP(DVB-EVIMC12). Additionally, no evident differences in isosteric heats of adsorption were observed between these two polymers (Fig. S13 †), which indicated no apparent change occurred in the interaction between the polymers and targeted gas after hypercrosslinking treatment. The enhanced CO₂ uptake capacity of HP(DVB-EVIMC12) was attributed to its improved pore structure. The CO₂ uptake capacity of HP(DVB-EVIMC12) (24.22 and 33.20 mg g⁻¹ at 25 and 0 °C, respectively) was higher than that of imidazolium-type MPILs reported in the literature (approximately 27.42 mg g⁻¹ at 0 °C and 1 bar).¹³

Selective separation of tocopherol homologues and organic phenolic compounds

The prepared MPILs exhibited selective separations for bioactive compounds and organic compounds with similar structures. Tocopherols are important fat-soluble vitamins in the biological system and act as effective antioxidants to scavenge free radicals. However, highly biologically active α-tocopherol is always accompanied by three other tocopherol homologues (*i.e.*, β-, γ-,

and δ-tocopherols). Therefore a key step in the production of high-purity α-tocopherol is the selective separation of α-tocopherol from these homologues.^{64–67} However this separation is very challenging due to their high structural similarities as displayed in Fig. 6A. Encouragingly, the distinct hydrogen-bond acidities follow the ascending order α-tocopherol < β- and γ-tocopherol < δ-tocopherol, which are expected to guide the difficult separation process.

The adsorption performance of P(DVB-EVIMCm)s was investigated by batch experiments with tocopherol homologues as typical bioactive solutes. As presented in Figs. 6B and C, all P(DVB-EVIMCm)s showed large adsorption capacities for tocopherols and high selectivities to homologues. Their performances were significantly superior to commercial adsorbents and P(nDVB-IL)s with common IL moieties. For example, the adsorption capacities of tocopherols on P(DVB-EVIMC12) were up to 211.45 mg g⁻¹ at 25 °C, which is 3.35 and 2.17 times larger than that for commercial resin adsorbents, Amberlite XAD-4 (63.21 mg g⁻¹) and Amberlite 717 (97.49 mg g⁻¹) as adsorbents, respectively. This was also significantly larger than the adsorption capacities of P(nDVB-IL)s with common ILs, such as P(2DVB-EVIMTf₂N) (96.67 mg g⁻¹), P(2DVB-EVIMBr) (106.81 mg g⁻¹), P(2DVB-EVIMPF₆) (119.34 mg g⁻¹), and P(2DVB-EVIMBF₄) (148.61 mg g⁻¹). Common MPILs, such as P(2DVB-EVIMBF₄), had a higher porosity (S_{BET}, 374 m² g⁻¹; V_{total}, 0.446 cm³ g⁻¹) than that of P(DVB-EVIMC12). However, P(DVB-EVIMC12) still demonstrated significantly higher adsorption capacities for tocopherols (211.45 mg g⁻¹ vs. 148.61 mg g⁻¹). Similarly, P(2DVB-EVIMBr) (S_{BET}, 371 m² g⁻¹; V_{total}, 0.271 cm³ g⁻¹) showed relatively lower tocopherol uptake (106.81 mg g⁻¹). LCC-ILs serve as stronger hydrogen-bond acceptors than common ILs and own great affinity for tocopherols,^{36, 68} which are scarce in these commercial resin adsorbents. Therefore, the introduction of functional carboxylate anions into MPILs significantly enhanced its adsorption capacity for

bioactive compounds. Moreover, the regeneration experiments showed that P(DVB-EVIMCm)s preserves its tocopherol adsorption capacity after four adsorption/desorption cycles (Fig. S15[†]).

Anion-functionalized MPILs exhibited very high adsorption capacities for tocopherols, and demonstrated extraordinary selectivity for different homologues. As shown in Fig. 6C, the selectivity of P(DVB-EVIMC12) for δ -tocopherol to α -tocopherol ($S_{\delta/\alpha}$) and for β - and γ -tocopherol to α -tocopherol ($S_{\beta\&\gamma/\alpha}$) were up to 8.65 and 4.20, respectively. Striking differences in the selectivity were observed among P(DVB-EVIMCm)s, commercial adsorbents, and common MPILs. The $S_{\delta/\alpha}$ and $S_{\beta\&\gamma/\alpha}$ values of the two resins were less than 1. P(nDVB-IL)s with common ILs also have poor separation selectivity. For example, the $S_{\delta/\alpha}$ and $S_{\beta\&\gamma/\alpha}$ values of P(2DVB-EVIMBr) were low at 2.36 and 1.58, respectively, and for P(2DVB-EVIMTf₂N), these values were as low as 1.52 and 1.20, respectively, which were distinctly inferior to those of all P(DVB-EVIMCm)s (Fig. 6C). To the best of our knowledge, P(DVB-EVIMC12) demonstrated the highest selectivity for tocopherol homologues among commercial adsorbents and reported porous materials. The excellent molecular selectivity of anion-functionalized MPILs for tocopherol homologues was mainly attributed to the strong hydrogen-bond basicity of incorporated long chain carboxylate anions in the polymers.^{36, 64, 68, 69}

Additionally, HP(DVB-EVIMC12) demonstrated a similar tocopherol adsorption performance (211.98 mg g⁻¹ with $S_{\delta/\alpha}$ and $S_{\beta\&\gamma/\alpha}$ values of 8.05 and 4.12, respectively) as that of the precursors of P(DVB-EVIMC12). This is because the adsorption of tocopherols on MPILs primarily depends on the nature and composition of the incorporated LCC-ILs, whereas the hypercrosslinking process gives rise to more abundant porosity without significantly changing the composition.

Furthermore, P(DVB-EVIMCm)s also showed excellent adsorption and separation performance for organic phenolic compounds, such as phenol, *p*-cresol, and 2,6-dimethylphenol, which have similar molecular structures shown in Fig. S16A[†]. As is well-known, phenol, *p*-cresol and 2,6-dimethylphenol are important feedstocks and intermediates in the chemical industry, and are mostly derived from coal tar oil as a mixture. As shown in Figs. S16B and C, P(DVB-EVIMCm)s exhibited very high adsorption capacities for the mixture of the above mentioned phenols with the values ranging from 279.32 to 305.61 mg g⁻¹. These values were larger than commercial adsorbents, such as Amberlite XAD-4 (107.76 mg g⁻¹) and P(nDVB-IL)s with common ILs, such as P(2DVB-EVIMTf₂N) (141.12 mg g⁻¹), P(2DVB-EVIMPF₆) (193.64 mg g⁻¹), P(2DVB-EVIMBr) (205.70 mg g⁻¹), and P(2DVB-EVIMBF₄) (240.13 mg g⁻¹). Significantly, for P(DVB-EVIMCm)s, the selectivity of phenol to 2,6-dimethylphenol ($S_{\text{phenol}/2,6\text{-dim}}$) and the selectivity of *p*-cresol to 2,6-dimethylphenol ($S_{p\text{-cresol}/2,6\text{-dim}}$) were both higher than those of common MPILs. For instance, excellent selectivities were realized even up to 9.49 ($S_{\text{phenol}/2,6\text{-dim}}$) and 6.12 ($S_{p\text{-cresol}/2,6\text{-dim}}$) with P(DVB-EVIMC12) as the adsorbent, respectively. However, the $S_{\text{phenol}/2,6\text{-dim}}$ and $S_{p\text{-cresol}/2,6\text{-dim}}$ values of P(2DVB-EVIMBr) were low at 5.32 and 3.59, respectively.

Conclusions

In summary, we explored a facile methodology combining microphase separation and hypercrosslinking to prepare anion-functionalized MPILs. A new family of anion-functionalized MPILs containing LCC-ILs were prepared. These MPILs possessed stable, well-developed mesopores and adequate functional IL contents. The hypercrosslinking treatment stabilized/rebuilt labile collapsed mesoporous network and produced new micropores, as shown by improved surface area and enhanced gas adsorption capacity. Anion-functionalized MPILs demonstrated good CO₂ capture performance (P(DVB-EVIMC12): 28.18 mg g⁻¹ at 0 °C and 1 bar) and exhibited extraordinarily high adsorption capacities (*i.e.*, 211.45 mg g⁻¹ for tocopherols) and excellent selectivities (*i.e.*, $S_{\delta/\alpha}$ 8.65; $S_{\beta\&\gamma/\alpha}$ 4.20) over commercial adsorbents and common MPILs for bioactive tocopherol homologues and organic phenolic compounds with high structural similarities. The prepared anion-functionalized MPILs had well-defined pore structure and possessed unique molecular recognition abilities, which makes them competent candidates for advanced separations. Therefore, this study demonstrated the potential of anion-functionalized MPILs as advanced adsorbents and facilitated a textural engineering approach to the development of novel porous ionic materials for other applications.

Experimental

Preparation of LCC-ILs

LCC-ILs were prepared as follows.^{35-37, 53} First, 1-ethyl-3-vinylimidazolium bromide ([EVIM][Br]) was synthesized as described in the literature.⁷⁰ A mixture of 1-vinylimidazole (9.41 g, 0.10 mol) and a slight excess of bromoethane (14.17 g, 0.13 mol) were dissolved in 30 mL MeOH with stirring for 15 h at 55 °C. Crude [EVIM][Br] was obtained by removing the solvent and then washing with ethyl acetate three times. [EVIM][Br] white solid was obtained after drying for 24 h at 50 °C. Afterward, [EVIM][Br] was dissolved in deionized water and passed through a strongly basic anion-exchange resin (Dowex Monosphere 550A UPW; OH type). The eluted 1-ethyl-3-vinylimidazolium hydroxide ([EVIM][OH]) aqueous solution was mixed with equimolar amounts of long-chain fatty acids at room temperature for 24 h. Aqueous silver nitrate (AgNO₃) solution was used to confirm complete anion exchange and the concentration of [EVIM][OH] was determined by acid-base titration. After solvent removal by evaporation under reduced pressure at 50 °C, LCC-ILs were dried under high vacuum to remove trace water. Seven IL monomers were prepared using different fatty acids, including acetic acid, butyric acid, hexanoic acid, octanoic acid, decanoic acid, laurate acid, myristic acid, and palmitic acid. The chemical structures of these obtained ILs were ascertained by ¹H NMR and ¹³C NMR spectra (in the ES[†]).

Synthesis of P(nDVB-EVIMCm)s and P(nDVB-IL)s with common anions

Typical copolymerizations of DVB and LCC-ILs were conducted as follows. In a 50-mL Schlenk flask, 1.00 g of DVB crosslinker, 2.48 g of [EVIM][C₁₁COO] monomer, and 0.07 g of 2,2'-azobis(2-methylpropionitrile) (AIBN) initiator were added to 10 mL MeCN, and the solution was stirred at room temperature for 2 h. Then, the

mixture was deoxygenated for 20 min and backfilled with N₂, followed by vigorous stirring at 80 °C for 24 h. After cooling to room temperature, the sample was washed with a large amount of EtOH, and dried under vacuum at 65 °C for 24 h. Then, the resultant yellow powder was ground for further applications.

P(nDVB-IL)s with common ILs ([EVIM][Br], 1-ethyl-3-vinylimidazolium tetrafluoroborate ([EVIM][BF₄]), 1-ethyl-3-vinylimidazolium hexafluorophosphate ([EVIM][PF₆]), and 1-ethyl-3-vinylimidazolium bis(trifluoromethylsulfonyl)imide ([EVIM][Tf₂N]) were obtained under similar methods, except the P(nDVB-IL)s sample used a 2:1 DVB: ILs molar ratio. For [EVIM][Br], a mixture of ethyl acetate, EtOH and H₂O (volume ratio = 8:2:1) was used as the porogenic solvent. And the textural parameters of, N₂ adsorption/desorption isotherms and pore size distributions are shown in Table S8 and Fig. S14. †

Synthesis of HP(DVB-EVIMCm)s

In a typical run for HP(DVB-EVIMCm)s, 0.40 g of the precursor P(DVB-EVIMC12) was swollen using 20 mL of EtOH, followed by the addition of 0.02 g of anhydrous FeCl₃. Then, the mixture was deoxygenated by pumping for 20 min, and backfilled with N₂, and stirred for 24 h at 80 °C. The produced sample was washed with plenty of water and EtOH to remove the FeCl₃ and was dried under high vacuum at 65 °C for 24 h.

Gas adsorption experiments

Adsorption isotherms of CO₂ and N₂ were measured on an ASAP 2050 (Micromeritics) at 25 and 0 °C and from 0 to 1 bar. All samples were degassed at 100 °C for 12 h prior to the measurements.

Pure component isotherm data were fitted with the dual-Langmuir-Freundlich isotherm (DSLFI) model (equation 1) for the calculation of the isosteric heat and adsorption selectivity:

$$q = q_{A,sat} \frac{b_A p^{v_A}}{1 + b_A p^{v_A}} + q_{B,sat} \frac{b_B p^{v_B}}{1 + b_B p^{v_B}} \quad (1)$$

where P (kPa) is the pressure of the bulk gas at the equilibrium with the adsorbed phase; q (mol kg⁻¹) is the adsorbed amount at the equilibrium; $q_{A,sat}$ and $q_{B,sat}$ (mol kg⁻¹) are the saturation capacities of site A and B; b_A and b_B (kPa^{-v_A}) are the affinity coefficients of site A and B; and v_A and v_B are the Freundlich coefficients. The fitted parameter values are presented in Table S6. †

The adsorption selectivity for CO₂/N₂ separation was estimated using ideal adsorbed solution theory (IAST) (equation 2):⁷¹

$$S_{ads} = \frac{x_i / x_j}{y_i / y_j} \quad (2)$$

where x_i and x_j are the adsorption capacity of component i and j , and y_i and y_j are the gaseous molar fractions of i and j .

The isosteric heats of adsorption were calculated using Virial equations (equation 3 and 4) based on isotherms at two different temperatures (25 and 0 °C). The fitted curves and parameter values are presented in Table S7 and Fig. S12: †

$$\ln p = \ln N + \frac{1}{T} \sum_{i=0}^m a_i N^i + \sum_{i=0}^m b_i N^i \quad (3)$$

$$Q_{st} = -R \sum_{i=0}^m a_i N^i \quad (4)$$

where P (kPa) is the pressure of the bulk gas at the equilibrium; N (mg g⁻¹) is the adsorbed amount at the equilibrium; T (K) is the corresponding temperature; Q_{st} (KJ mol⁻¹) is the isosteric heat; R is the ideal gas constant, 8.314 J mol⁻¹ K⁻¹; and a_i and b_i are Virial parameters.

Batch adsorption experiments

The batch adsorption experiments were carried out as follows. For tocopherol homologues, 40.00 mg adsorbent and 20 mL heptane solution with a total tocopherol concentration of 3.54 mg mL⁻¹ (the concentration of δ -tocopherol at 0.50 mg mL⁻¹, β - and γ -tocopherol at 1.54 mg mL⁻¹ in total, and α -tocopherol at 1.50 mg mL⁻¹) were added to the conical flask and shaken in a thermostatic rotary shaker at 25 °C and 200 rpm for 24 h to achieve adsorption equilibrium. Then, samples were taken from the solution, and the concentrations of tocopherols were determined using high performance liquid chromatography (HPLC).⁶⁴ The adsorption capacity Q_i and selectivity of solute i versus j ($S_{i/j}$) were calculated by equations 5 and 6:

$$Q_i = \frac{(C_{ei} - C_{fi})V}{W} \quad (5)$$

$$S_{i/j} = \frac{C_{ei} - C_{fi}}{C_{ej} - C_{fj}} \quad (6)$$

Where Q_i (mg g⁻¹) is the uptake of solute i on the adsorbent; C_{ei} and C_{fi} (mg mL⁻¹) are the concentrations of solute i in feed and equilibrium solution, respectively; V (mL) is the volume of the heptane solution and W (g) is the weight of the adsorbent. The adsorption experiments were repeated at least three times. In the adsorption experiments for organic phenolic compounds, the heptane solution contained 1.00 mg mL⁻¹ phenol, 1.15 mg mL⁻¹ p -cresol, and 1.30 mg mL⁻¹ 2,6-dimethylphenol.

The regeneration experiments were carried out as follows. After achieving adsorption equilibrium each time, the adsorbent was filtered, added to the conical flask with 25 mL EtOH, and shaken in a thermostatic rotary shaker at 45 °C and 200 rpm for 8 h, this procedure was performed for five times to regenerate the adsorbent adequately. Then for next cycle, the adsorbent was dried under high vacuum at 65 °C for 12 h.

Acknowledgements

The research was supported by the National Natural Science Foundation of China (21222601, 21476192, and 21436010), the Zhejiang Provincial Natural Science Foundation of China (LR13B060001), and the Fundamental Research Funds for the Central Universities (2014XZZX003-17).

Notes and references

1. D. Wu, F. Xu, B. Sun, R. Fu, H. He and K. Matyjaszewski, *Chem. Rev.*, 2012, **112**, 565-567.
2. P. Kuhn, M. Antonietti and A. Thomas, *Angew. Chem. Int. Ed.*, 2008, **47**, 3450-3453.

3. J. Byun, S.-H. Je, H. A. Patel, A. Coskun and C. T. Yavuz, *J. Mater. Chem. A*, 2014, **2**, 12507-12512.
4. F. Liu, L. Wang, Q. Sun, L. Zhu, X. Meng and F. S. Xiao, *J. Am. Chem. Soc.*, 2012, **134**, 16948-16950.
5. P. Zhang, Z. A. Qiao, X. Jiang, G. M. Veith and S. Dai, *Nano Lett.*, 2015, **15**, 823-828.
6. J. Yuan and M. Antonietti, *Polymer*, 2011, **52**, 1469-1482.
7. J. Yuan, D. Mecerreyes and M. Antonietti, *Prog. Polym. Sci.*, 2013, **38**, 1009-1036.
8. S. Zhang, K. Dokko and M. Watanabe, *Chem. Sci.*, 2015, **6**, 3684-3691.
9. S. Yuan, Q. Deng, G. Fang, M. Pan, X. Zhai and S. Wang, *J. Mater. Chem.*, 2012, **22**, 3965-3972.
10. S. Zulfiqar, M. I. Sarwar and D. Mecerreyes, *Polym. Chem.*, 2015, **6**, 6435-6451.
11. D. Chandra and A. Bhaumik, *J. Mater. Chem.*, 2009, **19**, 1901-1907.
12. A. Wilke, J. Yuan, M. Antonietti and J. Weber, *ACS Macro Lett.*, 2012, **1**, 1028-1031.
13. S. Soll, Q. Zhao, J. Weber and J. Yuan, *Chem. Mater.*, 2013, **25**, 3003-3010.
14. K. Täuber, Q. Zhao, M. Antonietti and J. Yuan, *ACS Macro Lett.*, 2014, **4**, 39-42.
15. J. E. Bara, C. J. Gabriel, E. S. Hatakeyama, T. K. Carlisle, S. Lessmann, R. D. Noble and D. L. Gin, *J. Membr. Sci.*, 2008, **321**, 3-7.
16. X. Hu, J. Tang, A. Blasig, Y. Shen and M. Radosz, *J. Membr. Sci.*, 2006, **281**, 130-138.
17. Q. Zhao, P. Zhang, M. Antonietti and J. Yuan, *J. Am. Chem. Soc.*, 2012, **134**, 11852-11855.
18. Y. Xie, Z. Zhang, J. Tao, J. He, B. Han, T. Wu and K. Ding, *Angew. Chem. Int. Ed.*, 2007, **46**, 7255-7258.
19. X. Wang, Y. Zhou, Z. Guo, G. Chen, J. Li, Y. Shi, Y. Liu and J. Wang, *Chem. Sci.*, 2015, **6**, 6916-6924.
20. Q. Zhao, J. W. Dunlop, X. Qiu, F. Huang, Z. Zhang, J. Heyda, J. Dzubielia, M. Antonietti and J. Yuan, *Nat. Commun.*, 2014, **5**, 4293-4293.
21. Y. Xiong, J. Liu, Y. Wang, H. Wang and R. Wang, *Angew. Chem. Int. Ed.*, 2012, **51**, 9114-9118.
22. Y. Deguchi, Y. Kohno and H. Ohno, *Chem. Commun.*, 2015, **51**, 9287-9290.
23. C. Gao, G. Chen, X. Wang, J. Li, Y. Zhou and J. Wang, *Chem. Commun.*, 2015, **51**, 4969-4972.
24. C. Liang and S. Dai, *Chem. Mater.*, 2009, **21**, 2115-2124.
25. M. Seo and M. A. Hillmyer, *Science*, 2012, **336**, 1422-1425.
26. X. Feng, C. Gao, Z. Guo, Y. Zhou and J. Wang, *RSC Adv.*, 2014, **4**, 23389-23395.
27. D. Kuzmicz, P. Coupillaud, Y. Men, J. Vignolle, G. Vendraminetto, M. Ambrogio, D. Taton and J. Yuan, *Polymer*, 2014, **55**, 3423-3430.
28. X. Wang, J. Li, G. Chen, Z. Guo, Y. Zhou and J. Wang, *ChemCatChem*, 2015, **7**, 993-1003.
29. F. Liu, W. Kong, C. Qi, L. Zhu and F. S. Xiao, *ACS Catal.*, 2012, **2**, 565-572.
30. Y. Yue, R. T. Mayes, J. Kim, P. F. Fulvio, X. G. Sun, C. Tsouris, J. Chen, S. Brown and S. Dai, *Angew. Chem. Int. Ed.*, 2013, **52**, 13458-13462.
31. Y. Zhang, S. Wei, F. Liu, Y. Du, S. Liu, Y. Ji, T. Yokoi, T. Tatsumi and F. S. Xiao, *Nano Today*, 2009, **4**, 135-142.
32. S. Dutta, K. C. W. Wu and T. Kimura, *Chem. Mater.*, 2015, **27**, 6918-6928.
33. N. Li, M. Zheng, S. Feng, H. Lu, B. Zhao, J. Zheng, S. Zhang, G. Ji and J. Cao, *J. Phys. Chem. C*, 2013, **117**, 8784-8792.
34. J. Zhang, Z. A. Qiao, S. M. Mahurin, X. Jiang, S. H. Chai, H. Lu, K. Nelson and S. Dai, *Angew. Chem. Int. Ed.*, 2015, **127**, 4665-4669.
35. W. Jin, Q. Yang, Z. Zhang, Z. Bao, Q. Ren, Y. Yang and H. Xing, *Chem. Commun.*, 2015, **51**, 13170-13173.
36. X. Liu, Q. Yang, Z. Bao, B. Su, Z. Zhang, Q. Ren, Y. Yang and H. Xing, *Chem. Eur. J.*, 2015, **21**, 9150-9156.
37. Y. Xie, H. Xing, Q. Yang, Z. Bao, B. Su and Q. Ren, *ACS Sustainable Chem. Eng.*, 2015, **3**, 3365-3372.
38. X. Ni, H. Xing, Q. Yang, J. Wang, B. Su, Z. Bao, Y. Yang and Q. Ren, *Ind. Eng. Chem. Res.*, 2012, **51**, 6480-6488.
39. M. Blahušiak, Š. Schlosser and J. Marták, *Sep. Sci. Technol.*, 2013, **119**, 102-111.
40. L. Alonso, A. Arce, M. Francisco, O. Rodríguez and A. Soto, *AIChE J.*, 2007, **53**, 3108-3115.
41. A. Arce, M. J. Earle, H. Rodríguez, K. R. Seddon and A. Soto, *Green Chem.*, 2008, **10**, 1294-1300.
42. X. Cui, K. Chen, H. Xing, Q. Yang, R. Krishna, Z. Bao, H. Wu, W. Zhou, X. Dong and Y. Han, *Science*, 2016, **353**, 141-144.
43. A. Dani, E. Groppo, C. Barolo, J. G. Vitillo and S. Bordiga, *J. Mater. Chem. A*, 2015, **3**, 8508-8518.
44. Y. Luo, B. Li, W. Wang, K. Wu and B. Tan, *Adv. Mater.*, 2012, **24**, 5703-5707.
45. L.-B. Sun, Y.-H. Kang, Y.-Q. Shi, Y. Jiang and X.-Q. Liu, *ACS Sustainable Chem. Eng.*, 2015, **3**, 3077-3085.
46. L.-B. Sun, A.-G. Li, X.-D. Liu, X.-Q. Liu, D. Feng, W. Lu, D. Yuan and H.-C. Zhou, *J. Mater. Chem. A*, 2015, **3**, 3252-3256.
47. G. Kyriakopoulos, D. Doulia and E. Anagnostopoulos, *Chem. Eng. Sci.*, 2005, **60**, 1177-1186.
48. X. Zeng, H. Yao, M. Ning, Y. Fan, C. Wang and R. Shi, *J. Colloid Interface Sci.*, 2011, **354**, 353-358.
49. K. Aleksieva, X. Jing, M. W. Li, A. Sassi, Z. Pientka, Z. Zhang and K. Jerabek, *Polymer*, 2006, **47**, 6544-6550.
50. S. Xu, Y. Luo and B. Tan, *Macromol. Rapid Commun.*, 2013, **34**, 471-484.
51. M. Seo, S. Kim, J. Oh, S. J. Kim and M. A. Hillmyer, *J. Am. Chem. Soc.*, 2015, **112**, 297-311.
52. X. Zhao, Q. Yang, D. Xu, Z. Bao, Y. Zhang, B. Su, Q. Ren and H. Xing, *AIChE J.*, 2015, **61**, 2016-2027.
53. Q. Yang, D. Xu, J. Zhang, Y. Zhu, Z. Zhang, C. Qian, Q. Ren and H. Xing, *ACS Sustainable Chem. Eng.*, 2015, **3**, 309-316.
54. Q. Zhao, S. Soll, M. Antonietti and J. Yuan, *Polym. Chem.*, 2013, **4**, 2432-2435.
55. M. P. Tsyurupa and V. A. Davankov, *React. Funct. Polym.*, 2002, **53**, 193-203.
56. C. D. Wood, B. Tan, A. Trewin, F. Su, M. J. Rosseinsky, D. Bradshaw, Y. Sun, L. Zhou and A. I. Cooper, *Adv. Mater.*, 2008, **20**, 1916-1921.
57. Z. A. Qiao, S. H. Chai, K. Nelson, Z. Bi, J. Chen, S. M. Mahurin, X. Zhu and S. Dai, *Nat. Commun.*, 2014, **5**, 643-648.
58. L. Hu, H. Ni, X. Chen, L. Wang, Y. Wei, T. Jiang, Y. Lü, X. Lu and P. Ye, *Polym. Eng. Sci.*, 2016, **56**, 573-582.
59. J. Wang, Y. J. Wei, G. Yi and Y. Zhang, *Chem. Commun.*, 2015, **51**, 15708-15711.
60. A. Chinnappan and A. H. Tamboli, *Chem. Eng. J.*, 2015, **285**, 554-561.
61. J. Wang, W. Sng, G. Yi and Y. Zhang, *Chem. Commun.*, 2015, **51**, 12076-12079.
62. X. Wu, Y. Liu, Y. Liu, D. Di, M. Guo and L. Zhao, *RSC Adv.*, 2015, **5**, 72601-72609.

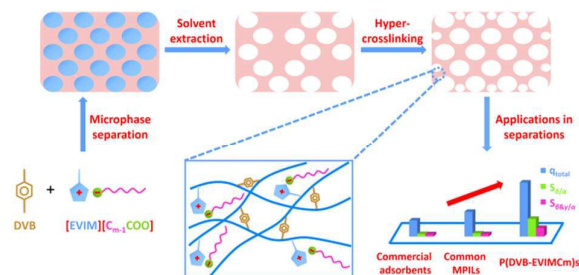
ARTICLE

Journal Name

63. J. Wang, L. Huang, R. Yang, Z. Zhang, J. Wu, Y. Gao, Q. Wang, D. O'Hare and Z. Zhong, *Energy Environ. Sci.*, 2014, **7**, 3478-3518.
64. Q. Yang, H. Xing, Y. Cao, B. Su, Y. Yang and Q. Ren, *Ind. Eng. Chem. Res.*, 2009, **48**, 6417-6422.
65. F. Bezold, M. E. Weinberger and M. Minceva, *J. Chromatogr. A*, 2017, **1491**, 153-158.
66. L. Qin, J. Zhang, H. Cheng, L. Chen, Z. Qi and W. Yuan, *ACS Sustainable Chem. Eng.*, 2016, **4**, 583-590.
67. H. Liu, G. Fang, C. Li, M. Pan, C. Liu, C. Fan and S. Wang, *J. Mater. Chem.*, 2012, **22**, 19882-19887.
68. Q. Yang, H. Xing, B. Su, Z. Bao, J. Wang, Y. Yang and Q. Ren, *AIChE J.*, 2013, **59**, 1657-1667.
69. J. Marták and Š. Schlosser, *Sep. Sci. Technol.*, 2007, **57**, 483-494.
70. J. Yuan and M. Antonietti, *Macromolecules*, 2011, **44**, 744-750.
71. A. L. Myers and J. M. Prausnitz, *AIChE J.*, 1965, **11**, 121-127.

View Article Online
DOI: 10.1039/C7TA01986F

Table of content



New anion-functionalized mesoporous poly(ionic liquid)s were synthesized *via* a microphase separation-hypercrosslinking strategy, and were utilized as highly efficient adsorbents for bioactive molecules.